Stability Analysis of a Hierarchical Lane-keeping Controller with Feedback Delay [★]

Illés Vörös [*] **Dénes Takács** [**]

[*] *MTA-BME Research Group on Dynamics of Machines and Vehicles, Budapest, H-1111, Hungary (e-mail: illes.voros@mm.bme.hu)*
[**] *Department of Applied Mechanics, Budapest University of Technology and Economics, Budapest, H-1111, Hungary (e-mail: takacs@mm.bme.hu)*

Abstract: A hierarchical lane-keeping controller of passenger cars is analyzed, with the consideration of feedback delay in the control loop. The higher-level controller generates the desired steering angle based on the delayed feedback of the lateral position and yaw angle of the vehicle. The feedback delay of the lateral position and the yaw angle are treated separately in the model, therefore more general sensor setups and estimation algorithms can be handled. A lower-level proportional-integral-derivative power steering controller ensures that the desired steering angle signal is followed properly. The linear stability analysis of the resulting closed-loop system is performed, with a focus on the controller parameters and the delay values. The optimal control gains, leading to the fastest decay of the solution are also investigated in detail. The results are showcased with the help of stability charts and numerical simulations.

Keywords: lane-keeping, steering control, feedback delay, multiple delays, stability analysis

1. INTRODUCTION

One of the fundamental aspects of automated driving functions is the ability of the vehicle to follow a given path. It is a commonly used simplification to decouple the longitudinal and lateral dynamics of the vehicle, and design the corresponding controllers separately (Rajamani (2011), Beregi et al. (2021)). In this paper, the lateral controller is analyzed in detail, with the consideration of a hierarchical control scheme. The higher level controller uses the lateral position and yaw angle errors of the vehicle with respect to the reference path to generate a desired steering angle. A lower-level proportional-integral-derivative (PID) controller is then used to ensure that the actual steering angle matches the reference.

In order to avoid unwanted oscillations and stability issues, the time delay in the control loop has to be considered when selecting the control gains. In case of a steering controller, the main sources of the feedback delay are sensor and communication delays, the computation time of the estimation and control algorithms, and actuator delay (Heredia and Ollero (2007), Vörös and Takács (2022)). Typically, the delay of the lower-level controller, which is related to its sampling frequency is much smaller than the delay in the higher-level control loop. In Beregi et al. (2018), it was shown that as long as the lower-level feedback delay is below a critical value (≈ 1 ms), it has a negligible effect on the stability of the lane-keeping control, therefore in this paper, only the time delay of the higher-level control loop will be considered.

However, due to the different sensor setups and estimation algorithms, it is possible that not all state variables have the same delay in the higher-level controller. Therefore, the feedback delay of the lateral position and the yaw angle error will be treated separately in our analysis. By performing the linear stability analysis of the resulting time delay system with multiple delays, the effects of the different control parameters and delay values on the stability and performance of the closed-loop system will be highlighted. We show that in certain cases, it can even be beneficial to increase the feedback delay.

The rest of the paper is organized as follows: the vehicle model with the hierarchical steering controller is presented in Section 2 and the linear stability analysis of the closed-loop system is performed in Section 3. In Section 3.1, the critical characteristic exponents are investigated, in Section 3.2, the domains of stabilizing control gains are presented in stability charts, and in Section 3.3 the control gains leading to the fastest decay of the solution are investigated. The results are concluded in Section 4.

2. VEHICLE MODEL AND CONTROL DESIGN

In order to describe the lateral dynamics of the vehicle, we use the in-plane bicycle model as shown in Fig. 1. The model includes four generalized coordinates: x_R and y_R
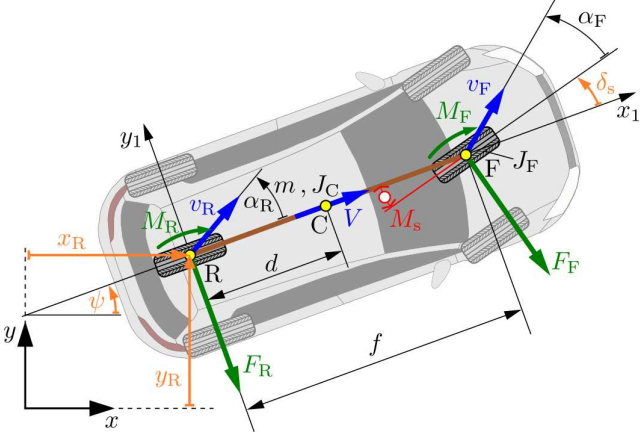
Fig. 1. Single-track vehicle model.

describe the position of the rear axle centerpoint (point R), ψ denotes the yaw angle and δ_s is the steering angle. The vehicle parameters include the wheelbase f, the distance d between the center of gravity (point C) and the rear axle, the vehicle mass m and the yaw moment of inertia J_C about the center of mass. The mass moment of inertia of the steering system is denoted by J_F.

The longitudinal speed of the rear wheel driven vehicle is assumed to be constant (V). This can be considered as a kinematic constraint in the model, which makes the system non-holonomic. The equations of motion are derived using the Gibbs–Appell method (Greenwood (2006)), but there are other methods available as well (see e.g. Bloch (2003) and Kane and Levinson (1985)). For the details of the derivation, see Vörös and Takács (2022).

The resulting equations for the time derivatives of the generalized coordinates are

$$\dot{x}_R = V \cos\psi - \sigma_1 \sin\psi\,, \tag{1}$$
$$\dot{y}_R = V \sin\psi + \sigma_1 \cos\psi\,, \tag{2}$$
$$\dot{\psi} = \sigma_2\,, \tag{3}$$
$$\dot{\delta}_s = \sigma_3\,, \tag{4}$$

where σ_1, σ_2 and σ_3 are the so-called pseudo-velocities, which are defined as the lateral velocity of point R, the yaw rate of the vehicle, and the steering rate, respectively. The rest of the equations of motion describe the dynamics of the pseudo-velocities as follows:

$$\begin{bmatrix} m & md & 0 \\ md & J_C + md^2 + J_F & J_F \\ 0 & J_F & J_F \end{bmatrix} \begin{bmatrix} \dot{\sigma}_1 \\ \dot{\sigma}_2 \\ \dot{\sigma}_3 \end{bmatrix} = \begin{bmatrix} f_1 \\ f_2 \\ f_3 \end{bmatrix}\,, \tag{5}$$

where the terms on the right-hand side are

$$f_1 = -F_R - F_F \cos\delta_s - mV\sigma_2\,, \tag{6}$$
$$f_2 = -M_F - M_R - F_F f \cos\delta_s - mdV\sigma_2\,, \tag{7}$$
$$f_3 = -M_F + M_s\,. \tag{8}$$

Here, M_s denotes the steering torque, F_F and F_R refer to the tire side forces, while M_F and M_R are the self-aligning moments at the front and rear wheels, respectively. Since the focus of this paper is the linear stability analysis of the system, the tire forces and self-aligning moments are modeled as linear functions of the side-slip angles α_F and α_R with coefficients C_i (cornering stiffness) and $\tilde{C}_i$:

$$F_i = C_i \alpha_i\,, \quad M_i = -\tilde{C}_i \alpha_i\,, \quad i \in \{F, R\}\,. \tag{9}$$

The side-slip angles are calculated as follows:

$$\alpha_F = \arctan\left(\frac{(\sigma_1 + f\sigma_2)\cos\delta_s - V\sin\delta_s}{(\sigma_1 + f\sigma_2)\sin\delta_s + V\cos\delta_s}\right)\,, \tag{10}$$
$$\alpha_R = \arctan\left(\frac{\sigma_1}{V}\right)\,. \tag{11}$$

Next, we design a feedback controller for lane-keeping to allow stable path following of the vehicle. For the stability analysis of the closed-loop system, a straight-line reference path along the x axis is considered. In order to better handle more complex curvatures, the feedback controller can be extended with a feedforward term, as in e.g. Qin et al. (2021).

We use a hierarchical controller design, where the higher-level control loop generates the desired steering angle (δ_s^{des}) based on the delayed feedback of the lateral deviation and the yaw angle error:

$$\delta_s^{des}(t) = -P_y y_R(t - \tau_y) - P_\psi \psi(t - \tau_\psi)\,. \tag{12}$$

Depending on the sensor configuration and the estimation methods used in the vehicle, the feedback delay of y_R and ψ might not be the same in practice, therefore we use the notation τ_y and τ_ψ to differentiate them. In addition, P_y and P_ψ represent the corresponding control gains.

The resulting desired steering angle from the higher-level control law in Eq. (12) is then used as the reference signal of the lower-level controller, which generates the steering torque M_s. Here, a PID controller of the form

$$M_s = -k_p\left(\delta_s - \delta_s^{des}\right) - k_d\sigma_3 - k_i z \tag{13}$$

is used, where k_p, k_d and k_i represent the control gains, and the integral of the error is considered using the additional state variable

$$\dot{z} = \delta_s - \delta_s^{des}\,. \tag{14}$$

In order to simplify the calculations, the reference steering rate is assumed to be zero. The numerical values of the lower-level control gains and J_F used in this paper are based on Beregi et al. (2021) (see Table 1).

3. STABILITY ANALYSIS

Since a straight-line reference path along the x axis is considered in our analysis, the lateral dynamics of the vehicle will not depend on the coordinate x_R, therefore it can be omitted. With the consideration of the integral state z, the state vector of the closed-loop system consists of

$$\mathbf{x} = [y_R\ \psi\ \delta_s\ \sigma_1\ \sigma_2\ \sigma_3\ z]^T\,, \tag{15}$$

and stable motion along the reference path corresponds to $\mathbf{x}(t) \equiv \mathbf{0}$. From the point of view of designing the higher-level controller, the linearized system around this equilibrium can be written as

$$\dot{\mathbf{x}} = \mathbf{A}\mathbf{x} + \mathbf{B}\delta_s^{des}\,, \tag{16}$$

where the desired steering angle is considered as the system input and the parameters of the lower-level controller are included in the state and input matrices:

$$\mathbf{A} = \begin{bmatrix} 0 & V & 0 & 1 & 0 & 0 & 0 \\ 0 & 0 & 0 & 0 & 1 & 0 & 0 \\ 0 & 0 & 0 & 0 & 0 & 1 & 0 \\ 0 & 0 & A_{43} & A_{44} & A_{45} & A_{46} & A_{47} \\ 0 & 0 & A_{53} & A_{54} & A_{55} & A_{56} & A_{57} \\ 0 & 0 & A_{63} & A_{64} & A_{65} & A_{66} & A_{67} \\ 0 & 0 & 1 & 0 & 0 & 0 & 0 \end{bmatrix}, \quad (17)$$

$$\mathbf{B} = [0 \ 0 \ 0 \ B_4 \ B_5 \ B_6 \ -1]^{\mathrm{T}}. \quad (18)$$

The elements of matrix $\mathbf{A}$ and $\mathbf{B}$ are listed in the Appendix. Using the control law in Eq. (12), the characteristic equation of the closed loop system is

$$D(\lambda) := \det\left(\lambda\mathbf{I} - \mathbf{A} - \mathbf{B}\left(\mathbf{K}_y e^{-\lambda\tau_y} + \mathbf{K}_\psi e^{-\lambda\tau_\psi}\right)\right) = 0, \quad (19)$$

where the row vectors $\mathbf{K}_y$ and $\mathbf{K}_\psi$ include the higher-level control gains in the appropriate positions:

$$\mathbf{K}_y = [-P_y \ 0 \ 0 \ 0 \ 0 \ 0 \ 0], \quad (20)$$

$$\mathbf{K}_\psi = [0 \ -P_\psi \ 0 \ 0 \ 0 \ 0 \ 0]. \quad (21)$$

Because of the time delays in the system, the characteristic equation is transcendental, with infinitely many roots for the characteristic exponent λ. At the stability boundaries, either a real characteristic exponent crosses the imaginary axis (static loss of stability, $\lambda = 0$) or a complex conjugate pair of characteristic roots move to the right half plane (dynamic stability loss, $\lambda = \pm i\omega$, where ω is the oscillation frequency at the stability boundary). Substituting $\lambda = 0$ into Eq. (19) leads to

$$D(0) = \frac{P_y k_i}{m J_F J_C}\left(C_F\left(\tilde{C}_R + f C_R\right) - \tilde{C}_F C_R\right) = 0. \quad (22)$$

This means (assuming realistic vehicle parameters) that static stability loss can occur at the control gains $P_y = 0$ and $k_i = 0$, regardless of the delay values.

3.1 Root tendencies

Figure 2 shows the real part of the rightmost characteristic roots as a function of the higher-level control gain P_y. The calculations were performed using the Matlab package DDE-Biftool (Engelborghs et al. (2001)). Black lines correspond to real characteristic roots, while blue lines represent complex conjugate pairs of roots. In order to better understand the effects of the integral action in the lower-level controller, Fig. 2(a) shows a simplified system without the integrator. In this case, the last term of the lower-level control law in Eq. (13) is not present (reducing to a PD controller), and the integral state z is not part of the state vector $\mathbf{x}$.

It can be seen that at the stability boundary of $P_y = 0$ (denoted as P_y^{fold} in Fig. 2), indeed a real characteristic exponent crosses the imaginary axis. As the value of P_y is increased inside the stable domain, the real part of the rightmost root decreases at first, indicating an improvement in control performance and stability. There exists an optimum (P_y^{opt}), where two real characteristic exponents merge. As P_y is further increased, these two exponents form a pair of complex conjugate roots. From this point on, the solution becomes oscillatory and control performance degrades as this complex pair of roots approaches the imaginary axis. Finally, the complex pair moves to the

Table 1. Vehicle parameters

Parameter	Value
Vehicle wheelbase (f)	2.7 m
Distance between rear axle and center of gravity (d)	1.35 m
Vehicle mass (m)	1430 kg
Yaw moment of inertia (J_C)	2500 kgm^2
Steering system moment of inertia (J_F)	0.25 kgm^2
Cornering stiffness of front wheels (C_F)	67000 N
Cornering stiffness of rear wheels (C_R)	50000 N
Self-aligning moment coefficient, front wheels ($\tilde{C}_F$)	1116.7 Nm
Self-aligning moment coefficient, rear wheels ($\tilde{C}_R$)	833.3 Nm
Lower-level steering control proportional gain (k_P)	640 Nm
Lower-level derivative gain (k_d)	8 Nms
Lower-level integral gain (k_i)	40 Nm/s
Longitudinal velocity (V)	20 m/s

right half-plane at the stability boundary P_y^{Hopf}, leading to a Hopf bifurcation in the nonlinear system.

When the integral term and the corresponding integral state z is introduced in the lower-level controller, an additional real characteristic root appears in the system, relatively close to the imaginary axis (see Fig. 2(b)). Although in most of the stable domain, this additional root resides closest to the imaginary axis, simulations show that the dominant system dynamics still behave according to the rest of the characteristic exponents, that remain largely in the same configuration as without the integral control. One slight change is that at the boundary of static loss of stability ($P_y = 0$), this new root crosses the imaginary axis instead of the original real λ. This change becomes more apparent as k_i is increased, as in Fig. 2(c).

3.2 Stability charts

In order to determine the boundaries of dynamic loss of stability in the planes of the different control gains, we used the D-subdivision method (Neimark (1949)). This involves substituting $\lambda = i\omega$ into the characteristic equation, separating the real and imaginary parts of the resulting complex equation, and solving the two equations for two system parameters. This leads to the curves of dynamic stability loss, parameterized by ω. These curves separate regions of the parameter plane with the same number of unstable characteristic roots. The stable parameter domain among the resulting stability boundaries can be identified using a number of methods: e.g. Stépán's formulae (Stépán (1989)), the semi-discretization method (Insperger and Stépán (2011)) or numerical simulations can all be applied to identify the stable region. For the results in this paper, the semi-discretization method was used.

First, the domains of stabilizing control gains of the lower-level controller were analyzed in Fig. 3. The higher-level gains in these stability charts were fixed at $P_y = 0.0095$ m^{-1} and $P_\psi = 0.56$, which corresponds to the fastest decay of the solution for the parameter set in Table 1. The stability charts show that increasing the
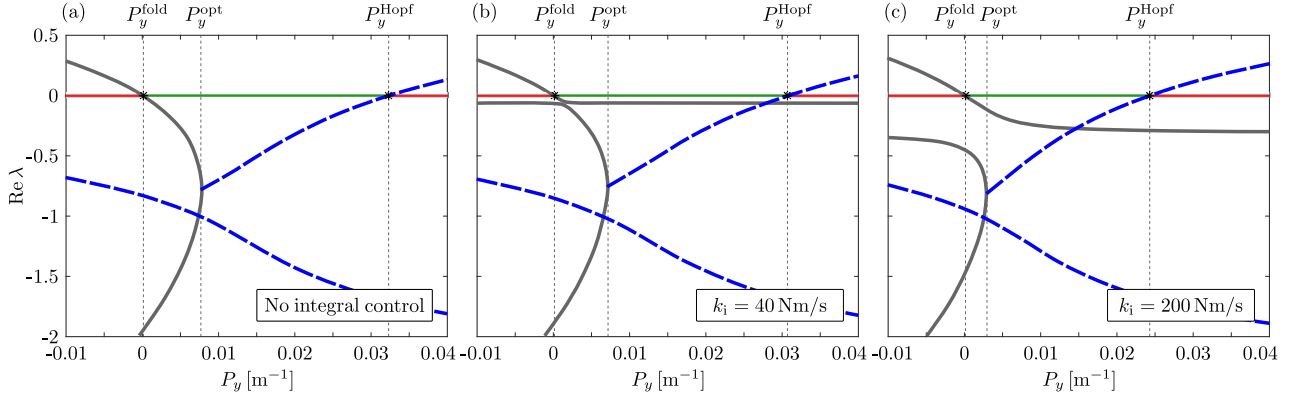
Fig. 2. The real parts of the rightmost characteristic roots as a function of the control gain P_y: (a) no integral action in the lower-level controller; (b) the integral gain is set to $k_i = 40$ Nm/s; (c) $k_i = 200$ Nm/s. Black continuous and blue dashed lines represent real and complex conjugate pairs of characteristic roots, respectively. The color of the stability boundary Re $\lambda = 0$ indicates the stable (green) and unstable (red) ranges of P_y. $P_\psi = 0.5$, $\tau_y = \tau_\psi = 0.5$ s and the rest of the parameters are listed in Table 1.
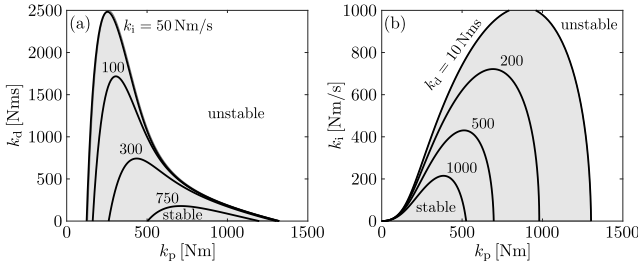

Fig. 3. Stable parameter domains of the lower-level controller for $P_y = 0.0095$ m^{-1}, $P_\psi = 0.56$ and $\tau_y = \tau_\psi = 0.5$ s. Vehicle parameters are listed in Table 1.

derivative gain k_d decreases the upper limit of the stabilizing values of k_p, while higher integral gains k_i mainly affect the lower bound of stable k_p values.

In Fig. 4, the stable domain of the higher-level control gains P_y and P_ψ are plotted for different amounts of feedback delay. It can be seen that increasing the delay of the yaw angle error leads to a sharp decrease in the size of the stable domain. On the other hand, increasing the feedback delay of the lateral deviation mainly affects the shape of the stable parameter domain. In certain cases, there even exist control gain combinations that turn from unstable to stable when τ_y is increased.

3.3 Optimal control gains

The optimal control gain combinations, leading to the fastest decay of the solution are also indicated in Fig. 4 (for the cases of $\tau_\psi = 0$, the optimum does not fall into the plotted region of the stability charts). As detailed in Section 3.1, the real part of the rightmost characteristic exponent (ignoring the one which corresponds to the integral state z) has the smallest value in these points. We used first order semi-discretization to determine these optimal points, by applying a step-size of $P_y = 5 \cdot 10^{-4}$ m^{-1} and $P_\psi = 5 \cdot 10^{-3}$ over the stable domain. The discretization size of the time delays was set to 0.01 s. The location of the optimal gain pairs show that achieving the fastest decay of the solution does not correspond to using the largest possible gain values. Especially in terms

of P_y, relatively smaller values lead to the best control performance, as explained by the root tendencies in Fig. 2.

The colormap in Fig. 5 shows how the real part of the critical characteristic exponent using the optimal control gains changes depending on the two delay values. This shows how close the system is to instability in the best-case scenario, with an optimally tuned controller. The optimal gains and the corresponding characteristic roots were evaluated for time delays between 0.05 s and 1 s with a step size of 0.05 s for both τ_y and τ_ψ. The calculations were performed using the semi-discretization method with the previously mentioned details.

Based on the critical real part corresponding to the optimal gains, the negative effects of increasing τ_ψ only become pronounced above ≈ 0.8 s. Above this level, a similar effect can be observed to what the stability charts in Fig. 4 suggested: namely, varying τ_y seems to have very little effect on the value of the critical real part, while further increasing τ_ψ leads to a sharp increase towards instability. Note, however, that the contour levels are becoming noisier as the size of the stable domain is decreasing, since the resolution of the P_y–P_ψ grid used during the calculations was not scaled with the stable region, which affects the accuracy of finding the optimum. In the region below $\tau_\psi = 0.8$ s, an opposite effect can be observed: increasing τ_y leads towards instability, but a higher value of τ_ψ can compensate this.

Figure 6 shows a pair of numerical simulations to further illustrate these counterintuitive results. In panel (a), the delay values were set according to point A in Fig. 5 ($\tau_y = 0.75$ s, $\tau_\psi = 0.25$ s), with the corresponding optimal gains of $P_y = 0.0105$ m^{-1} and $P_\psi = 0.82$. These result in a somewhat slow but smooth lane-change maneuver from the initial condition of $y(t \leq 0) = 3$ m (the rest of the state variables were set to zero). On the other hand, by increasing τ_ψ to 0.75 s in panel (b), the system (using the corresponding optimal gains of $P_y = 0.0065$ m^{-1} and $P_\psi = 0.41$) reaches the reference path significantly faster. Note that the control gains in the second case are considerably smaller, but they still lead to a more dynamic system response.
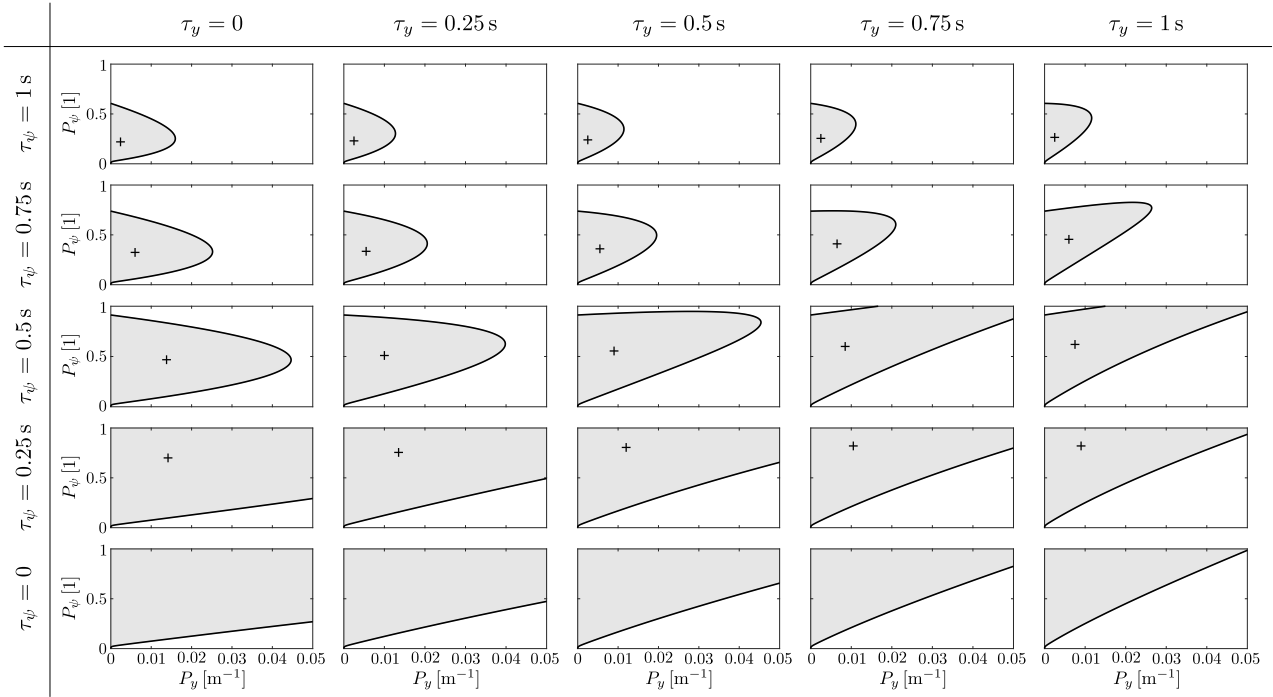
Fig. 4. The stable parameter domain of the higher-level control gains P_y and P_ψ for different amounts of feedback delay. The stable regions are shaded in gray. The optimal points in terms of the fastest decay of the solution are denoted by plus signs. Vehicle parameters are listed in Table 1.
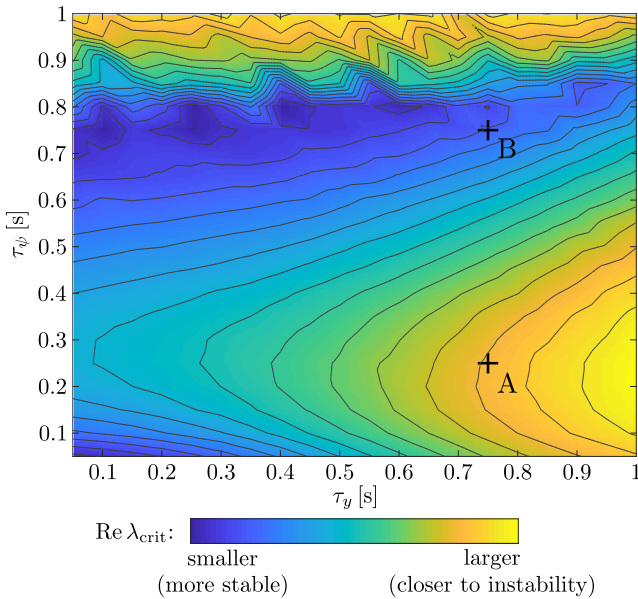

Fig. 5. The real part of the critical characteristic exponent using the optimal values of P_y and P_ψ as a function of the feedback delay τ_y and τ_ψ. Vehicle parameters are listed in Table 1.
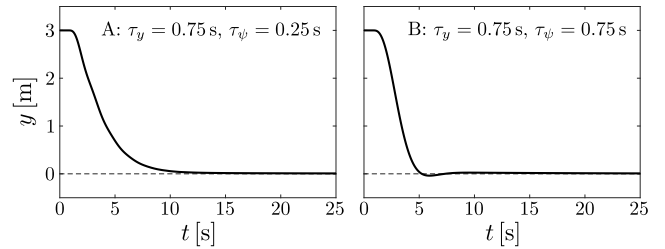

Fig. 6. Simulation results using the delay values in points A and B in Fig. 5 and the corresponding optimal control gains. Vehicle parameters are listed in Table 1.

to a faster system response and in some cases, increasing the feedback delay can be beneficial to improve control performance. These results can be used as guidelines when tuning the controllers in order to achieve reliable and safe path following of the vehicle.

4. CONCLUSION

A hierarchical lane-keeping controller with multiple delays was analyzed in this paper. With the help of stability charts, the domains of stabilizing control gains were identified for different combinations of feedback delay. In addition, the optimal control gains that lead to the most dynamic system response were also identified. We showed that a larger stable domain does not always correspond

REFERENCES

Beregi, S., Avedisov, S.S., He, C.R., Takacs, D., and Orosz, G. (2021). Connectivity-based delay-tolerant control of automated vehicles: theory and experiments. *IEEE Transactions on Intelligent Vehicles*.

Beregi, S., Takács, D., He, C.R., Avedisov, S.S., and Orosz, G. (2018). Hierarchical steering control for a front wheel drive automated car. *IFAC-PapersOnLine*, 51(14), 1–6.

Bloch, A.M. (2003). Nonholonomic mechanics. In *Nonholonomic mechanics and control*, 207–276. Springer.

Engelborghs, K., Luzyanina, T., and Samaey, G. (2001). Dde-biftool v. 2.00: a matlab package for bifurcation analysis of delay differential equations. *TW Reports*, 61–61.

Greenwood, D.T. (2006). *Advanced dynamics.* Cambridge University Press.

Heredia, G. and Ollero, A. (2007). Stability of autonomous vehicle path tracking with pure delays in the control loop. *Advanced Robotics*, 21(1-2), 23–50.

Insperger, T. and Stépán, G. (2011). *Semi-discretization for time-delay systems: stability and engineering applications*, volume 178. Springer Science & Business Media.

Kane, T.R. and Levinson, D.A. (1985). *Dynamics, theory and applications.* McGraw Hill.

Neimark, J. (1949). D-subdivisions and spaces of quasi-polynomials. *Prikladnaya Matematika i Mekhanika*, 13(5), 349–380.

Qin, W.B., Zhang, Y., Takács, D., Stépán, G., and Orosz, G. (2021). Dynamics and control of automobiles using nonholonomic vehicle models. *arXiv preprint arXiv:2108.02230.*

Rajamani, R. (2011). *Vehicle dynamics and control.* Springer Science & Business Media.

Stépán, G. (1989). *Retarded dynamical systems: stability and characteristic functions.* Longman Scientific & Technical.

Vörös, I. and Takács, D. (2022). Lane-keeping control of automated vehicles with feedback delay: Nonlinear analysis and laboratory experiments. *European Journal of Mechanics-A/Solids*, 104509.

$$A_{43} = \frac{C_{\mathrm{F}}(md(d-f) + J_{\mathrm{C}}) - mdk_{\mathrm{p}}}{mJ_{\mathrm{C}}},$$

$$A_{44} = \frac{(-\tilde{C}_{\mathrm{R}} - (C_{\mathrm{F}} + C_{\mathrm{R}})d + C_{\mathrm{F}}f)dm - (C_{\mathrm{F}} + C_{\mathrm{R}})J_{\mathrm{C}}}{mVJ_{\mathrm{C}}},$$

$$A_{45} = \frac{C_{\mathrm{F}}f(md(f-d) - J_{\mathrm{C}})}{mVJ_{\mathrm{C}}} - V,$$

$$A_{46} = -\frac{dk_{\mathrm{d}}}{J_{\mathrm{C}}},$$

$$A_{47} = -\frac{dk_{\mathrm{i}}}{J_{\mathrm{C}}},$$

$$A_{53} = \frac{C_{\mathrm{F}}(f-d) + k_{\mathrm{p}}}{J_{\mathrm{C}}},$$

$$A_{54} = \frac{(C_{\mathrm{F}} + C_{\mathrm{R}})d - C_{\mathrm{F}}f + \tilde{C}_{\mathrm{R}}}{VJ_{\mathrm{C}}},$$

$$A_{55} = -\frac{C_{\mathrm{F}}f(f-d)}{VJ_{\mathrm{C}}},$$

$$A_{56} = \frac{k_{\mathrm{d}}}{J_{\mathrm{C}}},$$

$$A_{57} = \frac{k_{\mathrm{i}}}{J_{\mathrm{C}}},$$

$$A_{63} = \frac{-\tilde{C}_{\mathrm{F}}J_{\mathrm{C}} - C_{\mathrm{F}}(f-d)J_{\mathrm{F}} - k_{\mathrm{p}}(J_{\mathrm{F}} + J_{\mathrm{C}})}{J_{\mathrm{F}}J_{\mathrm{C}}},$$

$$A_{64} = \frac{\left(-\tilde{C}_{\mathrm{R}} - (C_{\mathrm{F}} + C_{\mathrm{R}})d + C_{\mathrm{F}}f\right)J_{\mathrm{F}} + \tilde{C}_{\mathrm{F}}J_{\mathrm{C}}}{J_{\mathrm{F}}J_{\mathrm{C}}V},$$

$$A_{65} = \frac{f\left(C_{\mathrm{F}}J_{\mathrm{F}}(f-d) + \tilde{C}_{\mathrm{F}}J_{\mathrm{C}}\right)}{J_{\mathrm{F}}J_{\mathrm{C}}V},$$

$$A_{66} = -k_{\mathrm{d}}\frac{J_{\mathrm{F}} + J_{\mathrm{C}}}{J_{\mathrm{F}}J_{\mathrm{C}}},$$

$$A_{67} = -k_{\mathrm{i}}\frac{J_{\mathrm{F}} + J_{\mathrm{C}}}{J_{\mathrm{F}}J_{\mathrm{C}}}.$$

$$(A.1)$$

Matrix $\mathbf{B}$ in Eq. (18) includes

$$B_4 = \frac{dk_{\mathrm{p}}}{J_{\mathrm{C}}}, \quad B_5 = -\frac{k_{\mathrm{p}}}{J_{\mathrm{C}}}, \quad B_6 = k_{\mathrm{p}}\frac{J_{\mathrm{F}} + J_{\mathrm{C}}}{J_{\mathrm{F}}J_{\mathrm{C}}}. \quad (A.2)$$

Appendix A. COEFFICIENTS OF THE LINEARIZED SYSTEM

The elements of matrix $\mathbf{A}$ in Eq. (17) are the following: